


Selective targeting of nanomedicine to inflamed cerebral vasculature to enhance the blood–brain barrier

Oscar A. Marcos-Contreras^{a,1,2} , Colin F. Greineder^{a,1,2,3}, Raisa Yu Kiseleva^{a,1}, Hamideh Parhiz^{a,1}, Landis R. Walsh^a, Viviana Zuluaga-Ramirez^b, Jacob W. Myerson^a, Elizabeth D. Hood^a, Carlos H. Villa^a, Istvan Tombacz^c, Norbert Pardi^c, Alecia Seliga^b, Barbara L. Mui^d, Ying K. Tam^d, Patrick M. Glassman^a, Vladimir V. Shuvaev^{a,e}, Jia Nong^a, Jacob S. Brenner^{a,e,f}, Makan Khoshnejad^g, Tom Madden^d, Drew Weissmann^c, Yuri Persidsky^b, and Vladimir R. Muzykantov^{a,e,2}

^aDepartment of Systems Pharmacology and Translational Therapeutics, Perelman School of Medicine, University of Pennsylvania, Philadelphia, PA 19104; ^bDepartment of Pathology, Lewis Katz School of Medicine, Temple University, Philadelphia, PA 19140; ^cInfectious Diseases, Perelman School of Medicine, University of Pennsylvania, Philadelphia, PA 19104; ^dAcuitas Therapeutics, Vancouver, BC V6L 2A1, Canada; ^eCenter for Translational Targeted Therapeutics and Nanomedicine, University of Pennsylvania, Philadelphia, PA 19104; ^fPulmonary and Critical Care Medicine, Perelman School of Medicine, University of Pennsylvania, Philadelphia, PA 19104; and ^gThe Wistar Institute, Philadelphia, PA 19104

Edited by Kristi S. Anseth, University of Colorado Boulder, Boulder, CO, and approved December 31, 2019 (received for review July 15, 2019)

Drug targeting to inflammatory brain pathologies such as stroke and traumatic brain injury remains an elusive goal. Using a mouse model of acute brain inflammation induced by local tumor necrosis factor alpha (TNF α), we found that uptake of intravenously injected antibody to vascular cell adhesion molecule 1 (anti-VCAM) in the inflamed brain is >10-fold greater than antibodies to transferrin receptor-1 and intercellular adhesion molecule 1 (TfR-1 and ICAM-1). Furthermore, uptake of anti-VCAM/liposomes exceeded that of anti-TfR and anti-ICAM counterparts by ~27- and ~8-fold, respectively, achieving brain/blood ratio >300-fold higher than that of immunoglobulin G/liposomes. Single-photon emission computed tomography imaging affirmed specific anti-VCAM/liposome targeting to inflamed brain in mice. Intravital microscopy via cranial window and flow cytometry showed that in the inflamed brain anti-VCAM/liposomes bind to endothelium, not to leukocytes. Anti-VCAM/LNP selectively accumulated in the inflamed brain, providing de novo expression of proteins encoded by cargo messenger RNA (mRNA). Anti-VCAM/LNP-mediated expression of thrombomodulin (a natural endothelial inhibitor of thrombosis, inflammation, and vascular leakage) and alleviated TNF α -induced brain edema. Thus VCAM-directed nanocarriers provide a platform for cerebrovascular targeting to inflamed brain, with the goal of normalizing the integrity of the blood–brain barrier, thus benefiting numerous brain pathologies.

blood–brain barrier | cerebrovascular drug targeting | drug delivery to brain | mRNA therapy | VCAM-1

Drug delivery to the central nervous system (CNS) is an important and challenging goal. Strategies to achieve CNS delivery include local administration (1, 2), using cells and exosomes as carriers (3–7), and vascular drug targeting, that is, coupling drugs with affinity ligands for target molecules in the cerebral blood vessels. Ligands for transferrin receptor (TfR) (8), insulin receptor (9), P-selectin (CD62P) (10), intracellular adhesion molecule-1 (ICAM-1, or CD54) (11), and other targets have been used for cerebrovascular targeting (12, 13).

Most efforts in this area of research focus on drug delivery across the blood–brain barrier (BBB) via interventions including those transiently opening BBB or using BBB leakiness caused by the pathology (8–19). The BBB disruption is a hallmark of the pathogenesis of ischemic and hemorrhagic stroke, traumatic brain injury, meningitis, encephalitis, and other maladies. The BBB abnormalities also aggravate these pathologies by causing brain edema, inflammation, and tissue injury; hence, therapies normalizing the BBB integrity may improve management of these dangerous conditions, some of which lack effective pharmacotherapy (19, 20).

In this study, we set out to deliver drugs to the cerebrovascular endothelium, the key cellular constituent of the BBB, with the goal of normalizing and stabilizing the abnormal BBB. Animal studies showed that drug carriers (liposomes and lipid nanoparticles, LNPs) targeted to vascular cell adhesion molecule-1 (VCAM-1, or CD106) accumulate in the inflamed brain in more effectively and selectively than ICAM- and TfR-targeted counterparts. Furthermore, intravenous (i.v.) injection of VCAM-targeted LNPs carrying messenger RNA (mRNA) encoding for

Significance

Drug delivery to the brain is a challenging and elusive goal. Conjugating with ligands of target molecules including transferrin receptor modestly enhances cerebral accumulation of drugs and drug carriers. We found that conjugating with ligands of VCAM-1 provides order(s) of magnitude higher cerebral accumulation of nanocarriers, especially in the inflamed brain. VCAM-1 targeted nanocarriers loaded with messenger RNA encoding endothelial glycoprotein thrombomodulin cause expression of the transgene in the lumen of cerebral vasculature. This alleviates pathological permeability of the blood–brain barrier in mouse model of neurovascular inflammation. These results provide a basis for precise and effective molecular interventions in the cerebral vasculature.

Author contributions: V.R.M. conceived the study; V.R.M. directed the study; O.A.M.-C., C.F.G., R.Yu.K., L.R.W., P.M.G., J.N., J.S.B., D.W., Y.P., and V.R.M. designed research; O.A.M.-C., C.F.G., R.Yu.K., H.P., L.R.W., V.Z.-R., J.W.M., E.D.H., I.T., N.P., A.S., P.M.G., J.N., J.S.B., and M.K. performed research; V.R.M. organized the framework for the collaborative efforts; Y.K.T., T.M., D.W., and Y.P. directed part of the collaborative efforts; O.A.M.-C., R.Yu.K., H.P., V.Z.-R., J.W.M., E.D.H., C.H.V., I.T., N.P., B.L.M., Y.K.T., V.V.S., J.S.B., T.M., D.W., and Y.P. contributed new reagents/analytic tools; V.V.S. provided key knowledge; O.A.M.-C., C.F.G., R.Yu.K., L.R.W., V.Z.-R., J.W.M., C.H.V., P.M.G., Y.P., and V.R.M. analyzed data; B.L.M. and Y.K.T. provided a key reagent (LNPs); and O.A.M.-C., C.F.G., J.W.M., P.M.G., J.S.B., and V.R.M. wrote the paper.

Competing interest statement: O.A.M.-C., H.P., V.V.S., D.W., and V.R.M. are inventors on a patent filed on some aspects of this work. Those interests have been fully disclosed to the University of Pennsylvania.

This article is a PNAS Direct Submission.

Published under the [PNAS license](#).

¹O.A.M.-C., C.F.G., R.Yu.K., and H.P. contributed equally to this work.

²To whom correspondence may be addressed. Email: oscarmar@penmedicine.upenn.edu, coling@med.umich.edu, or muzykant@mail.med.upenn.edu.

³Present addresses: Department of Emergency Medicine and Department of Pharmacology, University of Michigan, Ann Arbor, MI 48109.

This article contains supporting information online at <https://www.pnas.org/lookup/suppl/doi:10.1073/pnas.1912012117/-DCSupplemental>.

First published January 31, 2020.

thrombomodulin (TM) transgene provided tangible alleviation of cerebrovascular edema induced by tumor necrosis factor alpha (TNF α). These results provide proof of concept for an approach normalizing pathologically altered BBB via targeted delivery of therapeutic mRNA to the abnormal cerebrovascular endothelium.

Results

Uniquely Selective and Effective Targeting of Anti-VCAM to the Inflamed Brain. To our knowledge, studies of VCAM-1-targeted drug delivery to the inflamed/activated BBB endothelium are lacking. To fill this gap of knowledge, here we embarked on the systematic quantitative analysis of the biodistribution parameters of candidate antibodies and a range of delivery systems, both at baseline and in a mouse model of TNF α -induced acute brain inflammation (by TNF α microinjection in the striatum).

Radiolabeled monoclonal antibodies against VCAM-1, ICAM-1, TfR-1, or control immunoglobulin G (IgG) were injected (0.2 mg/kg) i.v. in control mice and after microinjection of TNF α into the striatum. For each labeled antibody, in vitro immunoreactivity assays were performed prior to quantitative isotope tracing to ensure that a high percentage (>80%) retained antigen-binding activity (21). Fig. 1A shows data for the lungs (Fig. 1A, Left) and brain (Fig. 1A, Middle) of animals injected with anti-ICAM and anti-VCAM vs. control IgG. Comprehensive data for all ligands and organs for both groups of animals are given in *SI Appendix, Table S1*. This large-scale animal study unveiled intriguing and important findings.

In control mice, anti-ICAM demonstrated high pulmonary uptake ($109.9 \pm 9.2\%$ of the injected dose per gram of tissue; %ID/g, $P < 0.001$ vs. all other formulations), while uptake of anti-VCAM was an order of magnitude lower ($15.9 \pm 1.4\%$ ID/g). Uptake of anti-TfR was three times lower vs. anti-VCAM (4.7 ± 3.1 ; *SI Appendix, Table S1*), while that of control IgG was a further five times lower ($0.9 \pm 0.5\%$ ID/g). In contrast, brain uptake of anti-VCAM in control mice was on par with anti-TfR and four times higher than anti-ICAM (1.5 ± 0.1 vs. 1.7 ± 0.1 vs. $0.4 \pm 0.1\%$ ID/g, $P < 0.05$). Control IgG showed minimal brain uptake (0.1% ID/g, $P < 0.001$ vs. anti-VCAM).

Pulmonary uptake of anti-ICAM was further elevated in TNF α -challenged mice vs. naïve animals ($150.8 \pm 10.6\%$ ID/g). This presumably reflects an increase in pulmonary endothelial ICAM-1 and matches the well-documented interplay between brain injury and lung inflammation in humans (22). In contrast, anti-VCAM uptake in lungs of TNF α -challenged animals showed minimal change ($22.3 \pm 3.9\%$ ID/g), and pulmonary uptake of anti-TfR and untargeted IgG (5.1 ± 1.6 and $0.9 \pm 0.5\%$ ID/g, respectively; *SI Appendix, Table S1*) were not changed at all vs. control mice.

Most strikingly and importantly, the uptake of anti-VCAM increased more than an order of magnitude in the brain of TNF α -injured mice, far exceeding that of anti-ICAM and anti-TfR (17.1 ± 0.6 vs. $2.6 \pm 0.2\%$ and $1.5 \pm 0.2\%$ ID/g, anti-VCAM, anti-ICAM, and anti-TfR, respectively, $P < 0.001$). TNF α challenge did not affect IgG uptake in brain ($0.1 \pm 0.0\%$ ID/g, $P < 0.001$ vs. anti-VCAM). The time course of brain target accessibility is presented in *SI Appendix, Fig. S1*. Ratio of %ID/g in an organ and

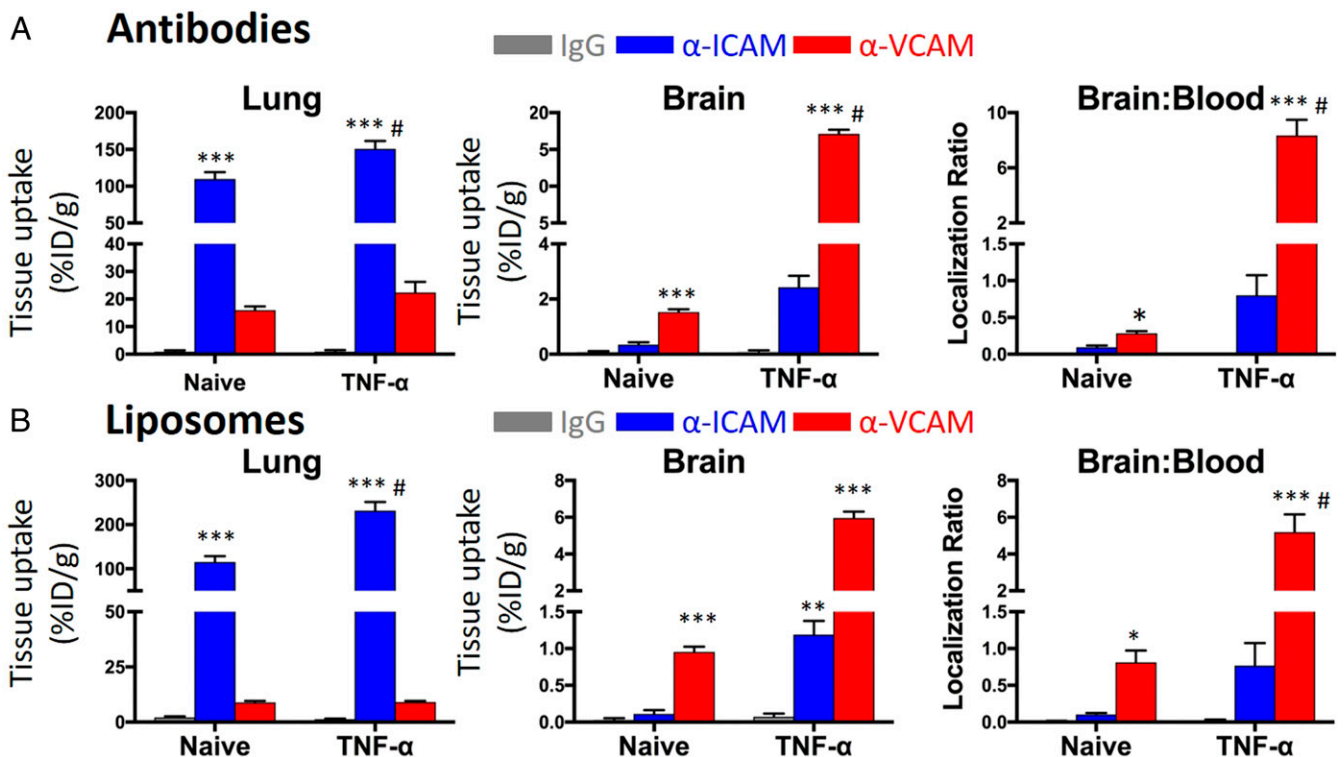


Fig. 1. Biodistribution of radiolabeled antibodies and immunoliposomes in naïve and TNF α -injured mice. (A, Left) Anti-ICAM-1 mAb demonstrates specific uptake in the lung ($***P < 0.001$ vs. IgG and VCAM-1), with a slight—but statistically significant—increase in animals receiving intrastriatal TNF α ($^{\#}P < 0.05$ vs. naïve). Anti-VCAM-1 mAb, in contrast, accumulates in the brain ($***P < 0.001$ vs. IgG and ICAM-1) and demonstrates a >10-fold increase in both brain uptake (A, Middle) and brain:blood ratio (A, Right) following intrastriatal TNF α ($***P < 0.001$ vs. naïve). (B) ICAM-1 and VCAM-1 targeted immunoliposomes show nearly identical patterns of lung and brain biodistribution as their counterpart mAbs. In particular, anti-VCAM-1 liposomes demonstrate a similar ~10-fold increase in brain uptake (B, Middle) and brain:blood ratio (B, Right) in TNF α -injured mice ($***P < 0.001$ vs. naïve). In all experiments, organ biodistribution was measured 30 min after i.v. injection (0.2 mg/kg of antibody and 20 mg/kg of liposome) of radiolabeled materials. mAb or immunoliposomes were given 16 h after intrastriatal TNF α injection. Each data point represents $n = 3$ animals with mean \pm SD shown, and two-way ANOVA with Dunnett's post hoc test was applied. Note that IgG and IgG/liposome bars are practically invisible in all panels (the data are shown in *SI Appendix, Table S1*). * $P < 0.05$ vs. IgG; ** $P < 0.01$ vs. IgG.

blood (localization ratio, LR, Fig. 1, *Right*) allows comparison of different formulations taking into account differences in blood clearance rate. In turn, dividing LR of a targeted formulation by LR of a nontargeted one yields the immunospecificity index (ISI; *SI Appendix, Table S1*). Analysis of these parameters helps one to appreciate the exquisite selectivity and efficacy of anti-VCAM targeting to the inflamed brain. The ISI of anti-VCAM uptake achieved $3,157.2 \pm 710.3$, indicating three orders of magnitude superiority over untargeted IgG, an order of magnitude over anti-ICAM-1 (ISI 273.3 ± 158.2) and more than two orders of magnitude over anti-TfR (ISI 14.6 ± 1.9).

Consistent with the kinetics of induction of expression of VCAM-1 and ICAM-1 in response to TNF α challenge that is known to take hours to reach the maximal expression (23, 24), targeting to these molecules was time-dependent, in contrast with the relatively stable and substantially inferior targeting to TfR (*SI Appendix, Fig. S3*).

Selective Targeting of Anti-VCAM/liposomes to the Inflamed Brain.

This study using antibodies identified VCAM-1 as a uniquely attractive target for inflamed brain. However, parameters of targeting of ligand-coated drug delivery vehicles often differ from those of free ligand, due to different pharmacokinetics and access and binding to the target, among other reasons. To appraise potential drug delivery utility of this finding, we reproduced this study using antibody-coated liposomes (20 mg/kg of liposomes), lipid-based nanocarriers that are among the most advanced translational carriers in nanomedicine. We employed site-specific click chemistry to conjugate antibodies to liposomes, labeled with ^{111}In bound to a diethylenetriaminepentaacetic acid (DTPA)-lipid to allow for direct tracing of the liposome. The characteristics of liposome formulations are summarized in *SI Appendix, Table S4*.

Intrigued by essentially opposite patterns of cerebral vs. pulmonary uptake of antibodies to VCAM-1 and ICAM-1, we focused on targeting liposomes to these two endothelial cell (EC) adhesion molecules (Fig. 1*B*). In general agreement with the behavior of the antibodies, anti-ICAM/liposomes accumulated extraordinarily well in the lungs and the uptake was further elevated in TNF α -striatum-challenged mice (115.6 and $231.7 \pm 19.5\%$ ID/g), whereas pulmonary targeting of anti-VCAM/liposomes did not exceed 10% ID/g in either control or TNF α -challenged mice and IgG uptake was in the range of 1 to 2% ID/g in both cases (Fig. 1*B, Left*).

In the brains of control mice, the uptake of anti-VCAM/liposomes exceeded that of anti-TfR/liposomes (0.2 ± 0.0) by four times and that of anti-ICAM/liposomes and IgG/liposomes (0.9 ± 0.1 vs. 0.1 ± 0.0 vs. $0.04 \pm 0.03\%$ ID/g, $P < 0.001$ anti-ICAM and IgG/liposomes vs. anti-VCAM/liposomes) by an order of magnitude (Fig. 1*B, Middle*). Furthermore, in mice with TNF α -induced acute brain inflammation, cerebral uptake of anti-VCAM/liposomes reached $6.0 \pm 0.3\%$ ID/g, vs. 1.2 ± 0.2 and $0.1 \pm 0.0\%$ ID/g for anti-ICAM/liposomes and IgG/liposomes, respectively (anti-ICAM and IgG/liposomes vs. anti-VCAM/liposomes, $P < 0.001$). The ISI of anti-VCAM/liposomes in the inflamed brain was 623.2 ± 401.6 , whereas ISI of anti-ICAM/liposomes was 20 times lower (36.3 ± 14.6 ; *SI Appendix, Table S2*).

In addition, sham-operated mice were included in our analysis. These animals were treated exactly as TNF α -injected counterparts (anesthesia, surgery, and intrastriatal injection) but received an injection of an equal volume of saline, rather than the inflammatory cytokine. We tested two parameters in these animals: 1) uptake of radiolabeled antibodies and IgG control (*SI Appendix, Table S3*) and 2) brain edema, as measured by leakage of radiolabeled albumin (see Fig. 6).

The uptake of IgG and anti-ICAM antibodies in sham-operated brain (ipsilateral hemisphere) was low and not statistically different from that seen in naïve animals ($0.15 \pm 0.07\%$ ID/g for IgG

sham ipsilateral vs. $0.08 \pm 0.04\%$ ID/g for IgG in naïve and $0.39 \pm 0.07\%$ ID/g for anti-ICAM sham ipsilateral vs. $0.35 \pm 0.08\%$ ID/g for ICAM in naïve, $P < 0.05$). In contrast, *SI Appendix, Table S3* shows that anti-VCAM antibody distribution was increased in the ipsilateral hemisphere of sham-operated animals ($2.36 \pm 0.10\%$ ID/g for sham ipsilateral vs. $1.52 \pm 0.10\%$ ID/g for naïve, $P < 0.05$), although the magnitude of this change was much smaller than that seen with TNF α -injected animals (17.10 ± 0.60 , $P < 0.001$ vs. naïve).

These results indicate that the sham procedure, not surprisingly, causes some degree of injury and inflammation and a corresponding increase in the amount of accessible VCAM-1 in the surrounding cerebrovasculature. Interestingly, the effect is not significant enough to allow leakage of nontargeted IgG into the brain tissue. This only further underlines the sensitivity of VCAM-1 biodistribution as a means of detecting brain pathology, a strategy detailed in prior reports (25–27), as well as its potential as a target for selective delivery of therapeutic cargo to areas of brain injury and inflammation.

Single-Photon Emission Computed Tomography /Computed Tomography Imaging of Cerebral Inflammation Using Anti-VCAM-1/liposomes.

VCAM-1 targeted particles have shown impressive results in imaging of brain inflammation and ischemia using MRI and other modalities in animals (25–28). Based on the encouraging magnitude of radiolabeled anti-VCAM/liposome uptake in the inflamed brain, we wanted to appraise potential imaging contrast utility of this formulation. Accordingly, we functionalized anti-VCAM/liposomes or IgG/liposomes with DTPA and loaded the chelate with ^{111}In . The ^{111}In -labeled liposomes were injected i.v. (20 mg/kg) in TNF-injured mice and the mice were imaged with single-photon emission computed tomography (SPECT) and computed tomography (CT) postmortem (Fig. 2*A* and *B*).

In contrast to IgG/liposomes, anti-VCAM/liposomes produced a strong signal in the inflamed brain tissue, with signal in the injured hemisphere predominant (Fig. 2*B*). Autoradiography of 2-mm brain slices from injured mice receiving anti-VCAM/liposomes confirmed the pattern of ^{111}In signal observed in SPECT images (Fig. 2*C*). Total background-corrected SPECT signal in the TNF-injured brain was sixfold higher in mice receiving anti-VCAM/liposomes, as compared to IgG/liposomes (Fig. 2*C*). As noted above, other studies have shown that VCAM-targeted nanoparticles can confer specific imaging contrast in injured brain vasculature. However, our result matches or exceeds previous state of the art in terms of VCAM specificity (25, 28), demonstrates VCAM-targeted imaging with SPECT, a quantitative imaging contrast modality (26, 27, 29), and employs liposomes, a nanoparticle with demonstrated biocompatibility and translational potential. Our results therefore confirm that VCAM-1 targeted nanoparticles can be used for noninvasive imaging of pathological vascular activation in brain pathology.

Of note, our imaging data indicate that VCAM up-regulation and targeting is distributed throughout the injured brain hemisphere. By contrast, a recent study by Llovera et al. (30) indicated that unilateral stroke will induce unilateral changes in the choroid plexus (CP), including possible CP-localized up-regulation of VCAM-1. Our finding of more distributed targeting may be attributable to differences between VCAM expression in TNF injury vs. stroke models, as indicated by findings with TNF injury in Montagne et al. (26) and with stroke models in Gauberti et al. (27).

Intravital Microscopy of Anti-VCAM/liposome Targeting to Inflamed Brain. Capitalizing on recent advances in intravital, multilabel fluorescent microscopy of cerebral vasculature in situ via cranial window (31), we imaged the real-time accumulation of anti-VCAM/liposomes in the inflamed brain. In order to induce inflammation of the superficial cerebral vessels, which can be

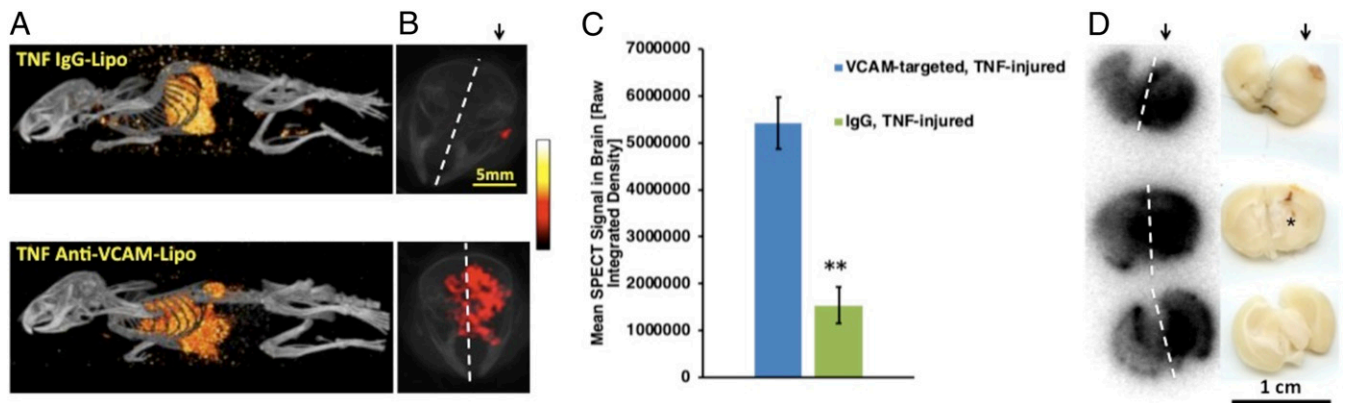


Fig. 2. SPECT imaging of immunoliposomes. Three-dimensional reconstructions (A) and average intensity projections (B) of SPECT (red) and CT (gray) signals for intrastriatal TNF α -injured mice receiving IgG or anti-VCAM-1 functionalized liposomes (20 mg/kg) bearing ^{111}In -DTPA ($n = 3$ per condition). Average intensity projections (B) encompassed SPECT and CT signal in the mouse cranium. (C) After Renyi filtering for noise removal, raw SPECT signal intensity was determined for a manually drawn field of view encompassing the cranial skull. Mean \pm SD ($n = 3$ per group); ** $P < 0.01$, t test. (D) Autoradiography images generated by anti-VCAM-1 functionalized liposomes bearing ^{111}In -DTPA in TNF α -injured brain sections. Arrows indicate the injected hemisphere, dashed lines delineate the brain hemispheres, and asterisk indicates injection site.

reliably imaged through the cranial window, TNF α microinjection was administered using a subarachnoid catheter. While no signal was observed at baseline, green fluorescent anti-VCAM/liposomes accumulated at the vascular margin within minutes of i.v. injection (20 mg/kg) in naïve mice (Fig. 3, *Left*), outlining bright large vessels in the area that is being imaged, which dims any signal from smaller vessels nearby.

Only occasional leukocytes (labeled with rhodamine dye) were seen passing through the vessels. The liposome signal faded and was no longer visible by 4 h postinjection. The attribution of vessels in this study is based on the analysis of their morphology (shape, size, branching, and vessel wall thickness) and relative flow rate (discernible in the real-time regimen of detection). Using these criteria we focused on the vessels that corresponded to post-capillary venules, because they 1) represent an important vascular segment controlling both vascular permeability and white blood

cells transmigration, 2) experience flow conditions less severe than arterial segment and therefore more permissive for following selected objects (leukocytes, liposomes, etc.), and 3) are more visually informative than capillaries, less visible at the resolution and magnification typical of the employed setup. For comparison, additional images of postcapillary venules (size 15 to 35 μm) are presented in *SI Appendix, Fig. S4*.

The same vessels were imaged after a second dose of anti-VCAM/liposomes (20 mg/kg) 24 h later and 2 h after localized injection of TNF α (Fig. 3, *Right*). In this case, the fluorescent signal was stronger and more prolonged, but the pattern was similar, outlining the vessel walls, consistent with endothelial localization. IgG/liposomes yielded very faint, if discernible at all, fluorescent signal from the cerebral vessels in both control and TNF α -challenged mice. We believe that the fluorescent dye staining detected in microvessels occurs due to the interaction of the

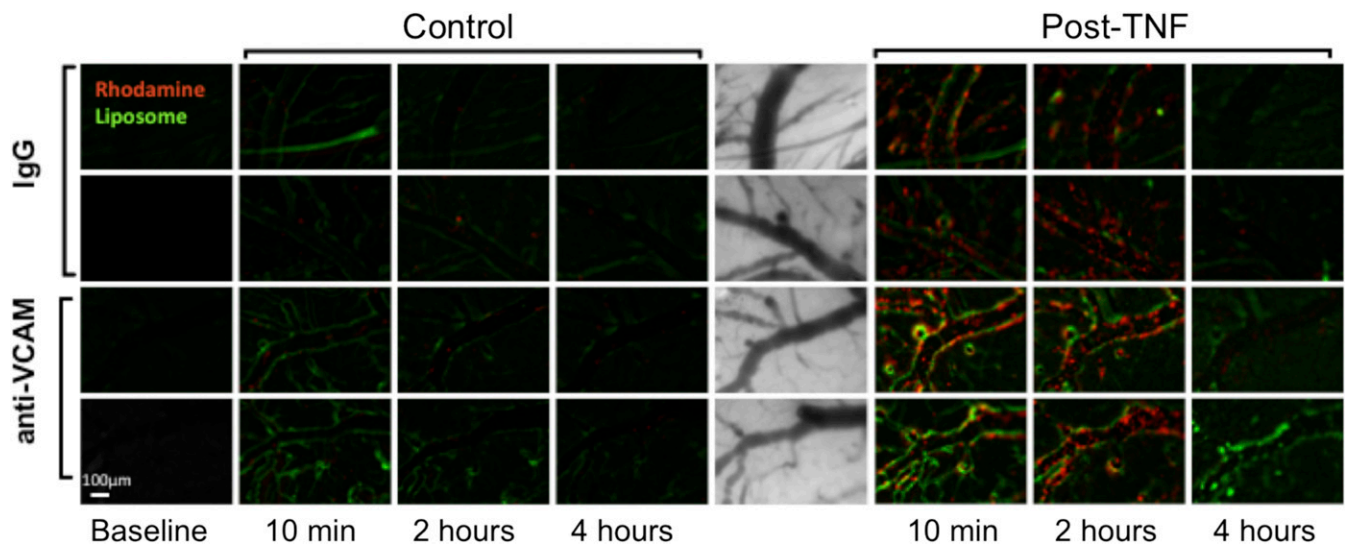


Fig. 3. Intravital imaging of cerebrovascular immunoliposome distribution. Intravital microscopy was performed through a cranial window and used to demonstrate real-time localization of fluorescent VCAM-1 targeted (bottom two rows, two independent animals) vs. IgG control (top two rows, two independent animals) liposomes (green; 20 mg/kg). Merged images also show circulating leukocytes (red) labeled via i.v. injection of rhodamine dye. Left-hand panels show baseline images and accumulation of liposomes 10 min, 2 h, and 4 h after administration in naïve mice (24 h prior to TNF α). Right-hand panels show the same three time points after administration of liposomes 2 h after TNF α injection in the same mice. Liposome uptake increases after TNF α injection, but localization remains predominantly at the vessel margin, despite a massive influx of circulating leukocytes.

liposomes with ECs. According to Jessen et al. (32), any solute that reaches the perivascular spaces is rapidly cleared out by the normal influx created by the arterial pulsations and is then driven deep into the parenchyma to be effluxed into the interstitial fluid. Indeed, our analysis at baseline clearly shows that there is no accumulation of fluorescence outside vessels.

Leukocytes were abundant in images of the post-TNF α -challenged cerebral vasculature (red color in the right images), yet relatively little colocalization was observed with anti-VCAM/liposomes. Indeed, by 4 h after liposome injection (6 h after TNF α infusion) there was essentially no new influx of rhodamine-labeled leukocytes, but the green fluorescent signal persisted in what appeared to be the brain endothelium.

Anti-VCAM and Anti-VCAM/liposomes Are Targeted Predominantly to Endothelial Cells in the Cerebral Vasculature. VCAM-1 is generally considered to be a more specific surface marker of activated ECs than ICAM-1, which is constitutively expressed and further up-regulated during pathology in many cell types (ECs, leukocytes, macrophages, and lymphocytes). Yet, studies that would directly attribute localization of VCAM-1 targeted agents to cell types *in vivo* are lacking.

Fluorescently labeled antibodies (0.2 mg/kg) or liposomes (20 mg/kg) were injected in control and TNF α -challenged mice and analyzed by flow cytometry in order to assess the cellular distribution of VCAM-1 targeted agents in the cell suspension obtained from brain homogenates. Cells were costained for CD31 and CD45 to identify target cell types: ECs (CD31⁺/CD45^{neg}), leukocytes (CD45^{Hi}), and microglial cells (CD45^{Mid}) (33). Double-negative cells, which stained for neither CD31 nor CD45, were not further subtyped. The relative percentage of each cell type was fairly consistent within each experimental group (i.e., control or TNF α -injected animals) but varied significantly between groups, with a much larger percentage of the cells recovered identified as leukocytes and microglial cells in the injured animals (Fig. 4 A and B).

Only a small percentage of ECs recovered from the brains of control mice stained positive for injected anti-VCAM monoclonal antibody (mAb) ($6.6 \pm 1.1\%$, vs. $0.06 \pm 0.02\%$ for IgG isotype control, $P < 0.001$; *SI Appendix, Fig. S2*). In contrast, i.v. injected anti-VCAM mAb stained more than half of ECs recovered from the brains of TNF α -injected animals ($51.6 \pm 1.6\%$, vs. $0.1 \pm 0.04\%$ for isotype control). The percentage of anti-VCAM-positive ECs was significantly higher than any other cell type: $10.3 \pm 0.7\%$ of leukocytes, $7.4 \pm 1.8\%$ of CD45^{Mid}, and $3.1 \pm 0.3\%$ CD31⁻/CD45⁻ double-negative cells ($P < 0.001$ for ECs vs. all other cell types). The mean fluorescence intensity (MFI) on VCAM-1 mAb-positive ECs was also significantly higher ($50,620 \pm 2,785$ arbitrary fluorescence units) as compared to other cell types ($12,380 \pm 403$ for leukocytes, $11,542 \pm 403$ for CD45^{Mid} cells, and $9,252 \pm 330$ for double-negative cells, $P < 0.001$ for ECs vs. all other cell types; *SI Appendix, Fig. S2*).

Similar results were seen for anti-VCAM/liposomes (Fig. 4 and *SI Appendix, Fig. S2*). Again, only a small percentage of ECs recovered from naïve mice ($4.9 \pm 0.9\%$, vs. $0.6 \pm 0.5\%$ for IgG control liposomes, $P < 0.001$) were found to be positive for anti-VCAM liposomes, whereas more than half of the ECs from TNF α injected animals were anti-VCAM liposome positive ($56.3 \pm 3.3\%$ vs. $1.3 \pm 1.2\%$ for IgG liposomes, $P < 0.001$). The percentage of positive ECs in TNF α -injected animals was significantly greater than leukocytes ($16.4 \pm 1.5\%$, $P < 0.001$), CD45^{Mid} cells ($14.3 \pm 3.9\%$, $P < 0.001$), and double-negative cells ($2.5 \pm 1.1\%$), and the MFI of anti-VCAM liposome-positive ECs was higher than that of the other cell types ($P < 0.001$ vs. leukocytes, CD45^{Mid}, and double-negative). Interestingly, $6.9 \pm 2.0\%$ of CD45^{Hi} leukocytes were found to be positive for IgG liposomes in TNF α -injected mice, as compared to only $1.3 \pm 0.4\%$ in naïve

mice ($P = 0.02$), indicating enhanced Fc-mediated uptake by infiltrating immune cells (*SI Appendix, Fig. S2*).

VCAM-Targeted LNPs Carrying TM mRNA Reduce TNF α -Induced Acute Brain Edema. Given the compelling results discussed above, namely the high degree of specific targeting of VCAM-1-targeted agents to inflamed cerebral ECs, we reasoned that this technology would be particularly well-suited to the delivery of a therapeutic with known activity in ECs. In particular, the endothelial surface glycoprotein TM is known to have critical roles in regulating coagulation, inflammation, and endothelial barrier function, and multiple previous studies in our laboratory have demonstrated its protective effects when targeted to the vascular endothelium (34, 35). Rather than anchor recombinant TM to the luminal membrane of the brain endothelium, a delivery strategy appropriate for noninternalizing surface targets (36), we utilized a method of targeted gene delivery (LNP mRNA) to induce *de novo* expression of TM by VCAM-1 expressing cerebrovascular endothelium (37, 38).

Before testing inducible TM expression, we studied the biodistribution of anti-VCAM/LNP. Specific anti-VCAM/LNP targeting to the inflamed brain resembled that of anti-VCAM/liposomes (*SI Appendix, Fig. S9*). As shown in Fig. 5A, cerebral uptake of radiolabeled anti-VCAM/LNP was >10 -fold higher than IgG/LNP in control mice and >70 -fold greater in TNF α -challenged mice (0.1 ± 0.0 vs. 1.1 ± 0.4 and 0.1 ± 0.0 vs. 7.6 ± 1.2). Likewise, anti-VCAM/LNP containing luciferase mRNA induced an almost fivefold higher level of the reporter signal in the brain of TNF α -challenged mice vs. anti-ICAM/LNP and IgG/LNP (Fig. 5B, dashed line represents IgG/LNP).

We next tested the expression of TM in brain following injection of anti-VCAM/LNPs loaded with TM mRNA (Fig. 5C and D and *SI Appendix, Figs. S5 and S6*). The TM transgene was tagged such that expressed protein would have a triple-flag tag fused to the cytoplasmic tail of the protein, allowing for straightforward determination of *de novo* expression vs. endogenous endothelial TM. Fig. 5C shows that mRNA loaded anti-VCAM/LNP, but not anti-ICAM/LNP, induced brain expression of TM when injected 17 h after TNF α injury (Fig. 5C and *SI Appendix, Fig. S5*). To compare LNP-induced TM expression in animals treated with TNF vs. control mice, we also traced appearance of accessible TM protein using i.v. injected radiolabeled anti-TM mAb (Fig. 5D). TM antibody uptake in the brain was quantified in naïve mice, TNF-injured mice, and TNF-injured mice after administration of VCAM-targeted LNPs bearing TM-encoding mRNA. Brain uptake of TM antibody did not differ between naïve mice and TNF-injured mice, but VCAM-targeted LNPs induced significantly higher levels of TM antibody accumulation in the brain vasculature.

Among other pathological changes typical of cerebral inflammation, TNF α insult also induces brain edema, which we measured by the tissue level of ^{125}I [albumin] leakage from blood (Fig. 6A). This quantitative readout of vascular permeability rose four times in TNF α -challenged animals relative to naïve controls (0.29 ± 0.08 vs. 1.17 ± 0.23 , phosphate-buffered saline [PBS]-injected vs. TNF α -injected animals) and remained unresolved for at least 2 d (*SI Appendix, Fig. S3*). We also tested the effect of sham operation on brain edema, as measured by the accumulation of radiolabeled albumin in the brain. Although leakage of untargeted IgG is not observed in these animals, the sham group does have significantly higher extravascular accumulation of radiolabeled albumin as compared to naïve mice (0.60 ± 0.15 for sham vs. 0.29 ± 0.08 , $P < 0.001$). These data are shown in Fig. 6A and used as comparators to calculate the percent of protection afforded by the LNP-TM therapeutic in Fig. 6B. In a double-blinded study, anti-VCAM/LNP-TM mRNA injected 17 h after TNF α significantly ($P < 0.001$) alleviated vascular leakage in the brain by $83.9 \pm 10.1\%$, but vascular leakage was not significantly reduced by

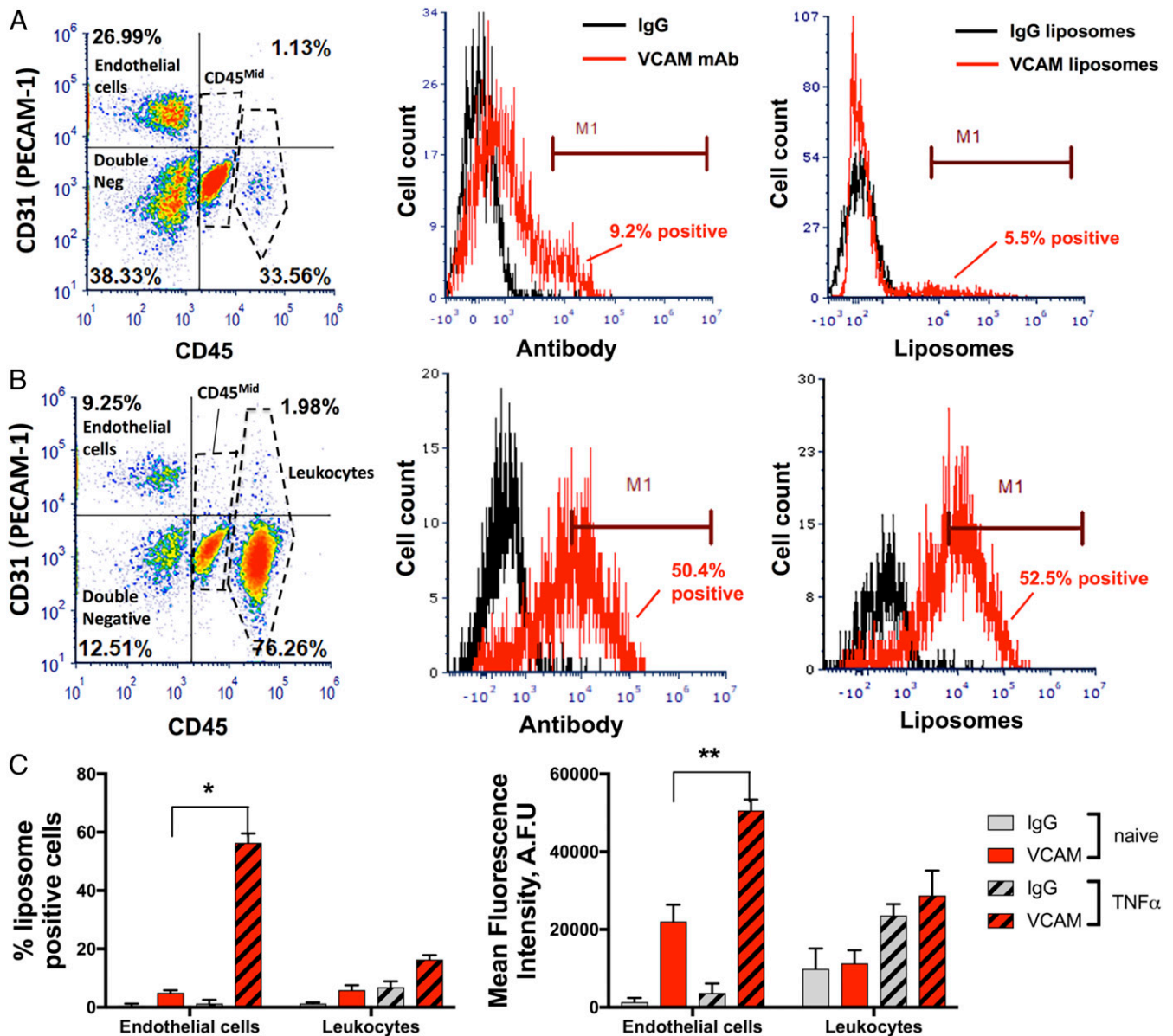


Fig. 4. Flow cytometric analysis of cell types involved in immunoliposome uptake. Flow cytometry was performed on disaggregated brains following injection of anti-VCAM-1 or IgG control immunoliposomes (20 mg/kg). CD31 and CD45 staining were used to identify four distinct cell populations: endothelial (CD45⁺CD31⁺), microglia/macrophages (CD45^{Mid}), leukocytes (CD45^{Hi}), and double-negative (CD45⁻CD31⁻) cells. Representative two-dimensional plots from naïve (A) and TNF α -injured mice (B) show identification of each cell type (Left), and histograms of far red staining, representing anti-VCAM antibody or IgG control positivity (Middle) or anti-VCAM liposome or IgG-liposome positivity (Right) in the EC gate. A minimum of 2×10^3 ECs was counted for all brains. (C) The percentage of liposome-positive ECs and leukocytes in control and TNF α -injured mice (Left) and the MFI of each cell type (Right) are summarized. While only a small percentage of ECs stain positive for anti-VCAM liposomes in control mice, more than half of recovered ECs are liposome-positive in TNF α -injured mice (* $P < 0.001$). A similar pattern is seen for the MFI, which is significantly higher in TNF α -injected vs. control mice (** $P < 0.001$). Each bar represents $n = 3$ mice with mean \pm SD shown, and brains were collected 30 min after injection.

identically administered untargeted counterpart LNP-TM mRNA (Fig. 6B). Importantly, the administration of different therapeutic mRNA (catalase and superoxide dismutase) failed to prevent albumin leakage (SI Appendix, Fig. S7).

Discussion

For decades the field of targeted drug delivery has tried to cross the BBB. Here we have refocused instead on targeting therapeutics to reside in the BBB and enhance the BBB's barrier function. Early BBB permeability has been identified as a key therapeutic target in a variety of brain injuries (20, 39). The idea of targeted therapeutic interventions restoring BBB functions,

proposed in this paper, is based on the current understanding of the mechanisms and pathological consequences of abnormally elevated permeability of the BBB caused by several common pathological processes including stroke, traumatic brain injury, and infectious diseases. In these pathologies, components of blood normally excluded from the brain parenchyma get access to its constituencies. These processes, manifested as accumulation of plasma proteins and blood cells in the brain (Figs. 4 and 6), are not innocuous. For example, extravasation of plasminogen activators leads to proteolysis in the tissue and proteolysis-bypassing direct and indirect proinflammatory signaling such as via interaction of regulatory domains of tPA and urokinase with cognate receptors

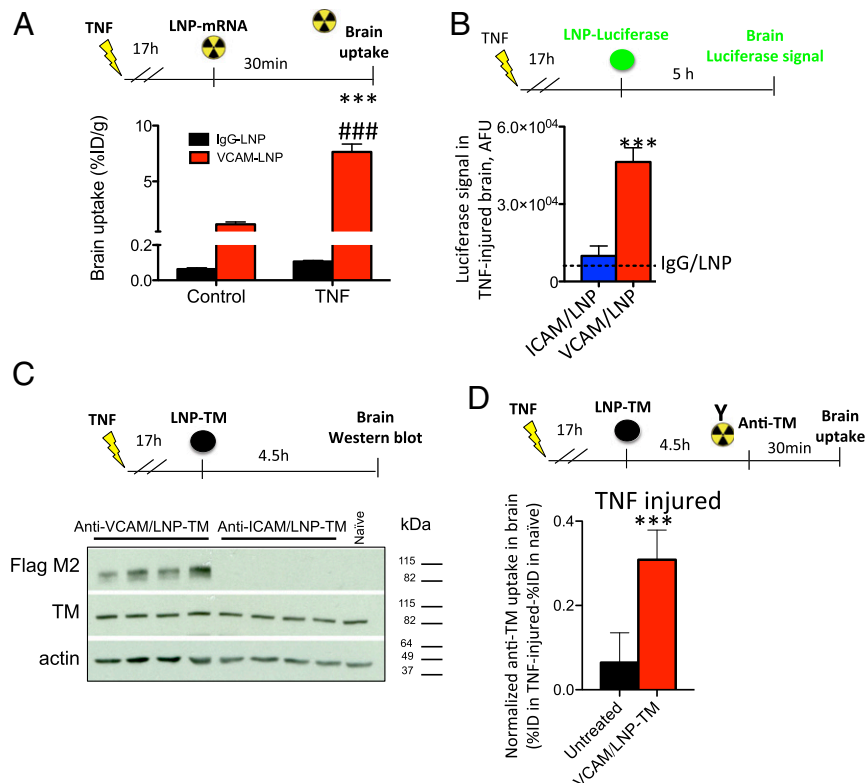


Fig. 5. Targeted LNPs accumulate in the brain and induce TM expression via mRNA delivery. (A) Ipsilateral brain uptake at 30 min after injection of ^{125}I -labeled anti-VCAM-1- and control IgG-LNPs (8 μg of mRNA) in healthy and intrastriatal TNF α -injured mice. Tissue uptake is indicated as mean \pm SEM ($n = 3$); tissue uptake of anti-VCAM-1-LNP was compared to IgG counterpart in both naïve and TNF α -treated mice ($***P < 0.001$, one-way ANOVA, Bonferroni post hoc). Anti-VCAM-1-LNP uptake was also compared in TNF α -treated mice vs. naïve mice ($####P < 0.0001$, one-way ANOVA, Bonferroni post hoc). Firefly luciferase expression (B) was measured in the ipsilateral hemisphere at 5 h after i.v. administration of anti-VCAM-1 and anti-ICAM-1-LNP-fluc mRNAs in TNF α -injured mice (dashed line indicates firefly luciferase luminescence induced by IgG-LNP-fluc mRNA). Luciferase transfection activity of anti-VCAM-1-LNP was compared to anti-ICAM-1-LNP ($***P < 0.001$, one-way ANOVA, Bonferroni post hoc). (C) Western blot for brain homogenates (10 μg total protein per lane) with staining for FLAG, TM, and α -actin. TNF α -injured mice ($n = 4$) were treated with anti-VCAM-1 (i.v. injected) and anti-ICAM-1 (administered via internal carotid artery) targeted LNPs bearing mRNA encoding for TM-FLAG (LNP-TM) 4.5 h after LNP treatment. (D) Normalized brain uptake (%ID/g in TNF-injured brain – %ID/g in naïve brain) of mAb against TM (5 μg of clone 411) 30 min after injection in TNF-injured animals (17 h after injury and 4.5 h after treatment with saline (Untreated) or VCAM/LNP-TM) (mean \pm SD; $n = 4$, t test: $***P < 0.001$).

on glial and neuronal cells (40). Red blood cells entering the CNS parenchyma are a source of free hemoglobin, a very damaging prooxidative agent in the tissue. Also, excessive extravasation of

host defense cells leads to tissue injury via multiple pathways. In theory, stabilization of the BBB may be substantially beneficial in these cases. Interventions alleviating the BBB dysfunction have

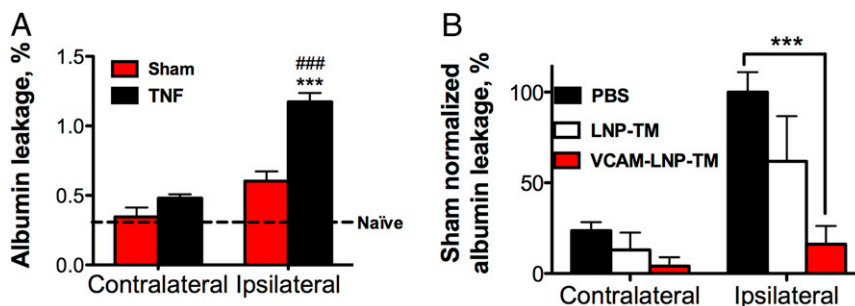


Fig. 6. Brain edema: extravascular radiolabeled albumin accumulation in the brain. (A) Assessment of brain edema using albumin leakage assay. Radiolabeled albumin was injected 21 h after unilateral striatal injection of TNF α (0.5 μg) and allowed to circulate for 4 h. The ratio between extravasated and bloodstream radiolabeled albumin was determined as counts per minute per gram of brain:counts per minute per gram of blood. Treatment with TNF α ($n = 14$) significantly increased albumin leakage in the ipsilateral hemisphere ($***P < 0.001$ in sham ipsilateral vs. TNF ipsilateral and $####P < 0.0001$ contralateral vs. ipsilateral in TNF injured and $P < 0.001$ TNF ipsilateral vs. naïve animals [$n = 6$], one-way ANOVA, Bonferroni post hoc). Data shown as mean \pm SEM. (B) Sham normalized albumin leakage, considering a 100% leakage as the value calculated for the ipsilateral hemisphere in PBS-treated animals and 0% leakage as the value calculated for the contralateral or ipsilateral hemisphere of the sham-operated animals. Treatment with anti-VCAM-1-targeted LNP-TM ($n = 6$) significantly reduced albumin leakage in ipsilateral hemisphere compared to nontargeted LNP-TM- ($n = 5$) and PBS vehicle- ($n = 8$) treated animals ($***P < 0.001$ vs. vehicle, one-way ANOVA, Bonferroni post hoc). Data shown as mean \pm SEM.

the ability to both prevent parenchymal injury and improve long-term functional outcome (41).

The protective effect of anti-VCAM/LNP carrying TM mRNA on brain edema is not unexpected, given the wealth of knowledge regarding the critical role of TM in maintaining barrier function (42, 43). We have documented antiedematous and antiinflammatory effects of pharmacologic augmentation of the endothelial protein C pathway targeted using ICAM-1 and PECAM-1 ligands to the pulmonary vasculature (34, 41, 44).

One reason that enhancing the BBB may have been understudied is that prior to the present study there were no good methods of targeting the BBB itself. We and others have devised technologies for targeted drug delivery to the endothelium (1, 34, 45–53). Constitutive endothelial surface markers, like PECAM-1, ubiquitously expressed at millions of copies per cell throughout the vasculature (46, 52), are attractive targets in systemic insults (e.g., sepsis). However, selective delivery to afflicted neurovascular units is preferable for treatment of localized CNS insults. Inducible cell-adhesion molecules, such as VCAM-1, which has been used as a marker of vascular inflammation in neurodegenerative diseases (26), stroke (27), encephalitis (54), and meningitis (55), represent more natural candidate targets for these applications.

Inducible cerebrovascular cell-adhesion molecules have been targeted as a therapeutic strategy in human CNS pathology. These studies focused on inhibition of leukocyte adhesion, rather than delivery of a therapeutic payload. For example, a murine antibody to human ICAM-1 (enlimomab), showing significant protective effects in animal studies, was tested in over 500 patients with ischemic stroke (56). The treatment was associated with toxicity and worsened clinical outcome, but subsequent studies have revealed that the adverse events in this trial were the result of complement activation by the murine IgG, rather than effect of binding to the target molecule, ICAM-1, that is expressed at high surface density in normal endothelium and further up-regulated in pathology (57, 58).

In contrast, VCAM-1 is expressed very selectively, although at relatively low levels, by abnormal endothelium (59). Accordingly, it is studied extensively as a candidate target for imaging applications, primarily for detection of vascular pathologies using positron emission tomography, SPECT, MRI, and optical and other imaging modalities (26–28, 60–62).

In particular, several studies proposed that VCAM-1 up-regulation in BBB endothelium may serve as an indicator of brain inflammation/endothelial activation, using VCAM-1 antibodies (multiple clones for mice and rats) as a way to target the inflamed brain for delivery of imaging probes. Our data showing accumulation of VCAM-targeted drug carrier formulations in the inflamed brain agree with the previous literature on VCAM targeting in inflammation. Notable previous work has shown that imaging probes conjugated to VCAM antibody clones including MK2.7, A429, and MR106 target the inflamed brain in diverse animal species (25–28). Taken together, our data and the literature indicate that the targeted drug delivery to the injured brain reported in the present study is due to VCAM-1 up-regulation in the BBB endothelium and may be achieved with different anti-VCAM clones. Liu et al. (25) used both MRI and fluorescence microscopy as a readout to show that liposomes presenting a VCAM-1 antibody will increase specificity to brain endothelium after ischemia (in a rat model of middle cerebral artery occlusion). Montagne et al. (26) also used both MRI and fluorescence microscopy and demonstrated that VCAM-1 antibodies conjugated to a contrast agent can be used as an imaging approach to identify brain inflammation (reasoning that VCAM-1 expression is an endothelial biomarker for activation). In this study, the TNF α inflammation induction model was used in mice. The same group [Gauberti et al. (27)] repeated this approach in ischemic and hemorrhagic strokes. Finally, Patel et al. (28) also used the TNF α

inflammation induction model, showing VCAM-1 antibody could provide injury-specific contrast in MRI and SPECT imaging.

The present work, however, is clearly distinct from these studies. In previous diagnostic imaging pursued by our predecessors, the primary priority was to achieve a discernible local signal typical of a pathological process, helping to identify the disease. In contrast, the key priorities in drug delivery pursued in our study include ratio of uptake in the target organ to that in other organs (e.g., brain to liver), the kinetics of drug delivery and postdelivery fate/activity of the pharmacological cargo (controlled by its release or/and interaction in the target), cellular and subcellular localization, the dose of drug delivered, and amplitude and duration of its effect. It might seem logical in retrospect that targeted drug delivery to VCAM-1—a selective yet scarce target—afforded no improvement in treatment of acute vascular inflammation in animal studies (63). Therefore, VCAM-1 targeted cerebrovascular pharmacological intervention documented in the present study represents the important outcome advancing the field of drug delivery to the brain.

In experiments aimed at real-time imaging of VCAM-targeted nanocarriers and leukocytes in the brain microvasculature using intracranial window microscopy, fluorescent signal must be monitored from a relatively shallow depth in the brain, due to its limited penetration of the tissues. Accordingly, in this experimental setting we administered TNF α via a subarachnoid catheter, in order to collect maximal signal from the affected area of the brain. This consideration also explains the differences in time interval used in each experimental setup. In each case, the time from TNF α challenge to outcome was chosen to achieve optimal conditions. In particular, a shorter period (2 to 6 h) after subarachnoid injection of TNF α was found to be optimal for visualization studies, as compared to 20 to 24 h after intrastriatal injection, which was found to be optimal for radiotracing studies.

These differences must be taken into consideration as a note that data of isotope tracing, fluorescent microscopy imaging, and protection studies are not fully and uniformly compatible. However, the goals and readouts of these settings are also different. Isotope tracing provides quantitative objective data of targeting and tissue uptake of the carriers in the brain with readouts fully compatible with other organs and studies, that is, percent of injected dose per organ or per gram of the organ (64). In contrast, fluorescent microscopy studies reveal the dynamics and localization of the particles and leukocytes in the brain microvasculature at micrometer-scale resolution. It is worth noting that each of these series unequivocally confirmed that VCAM-1 directed vascular immunotargeting to the brain vasculature is effective, specific, takes place in the brain microvasculature, and provides tangible benefits in acute brain inflammation.

The off-rate of these targeted agents represents an important topic. More precise and systematic kinetic studies are warranted to understand the dynamics of accumulation in the brain (and in other tissues), as well as dynamics of development of the effect for the agents that require additional time after delivery, such as some biologicals (nucleic acids, etc.). Most likely these dynamical factors will be different for specific pathological processes and formulations. For example, kinetics of delivery may be different in ischemic conditions. Further, cellular uptake and processing kinetics may differ between multivalent VCAM-targeted carriers and antibodies or monovalent fusions.

We have initiated pilot studies to characterize the off-rate and the duration of therapeutic effect for several formulations of targeted TM, in cell cultures and in mice. Our preliminary data indicate that, indeed, the dynamics of the effect is formulation-specific: TM directly conjugated with antibodies exerts effects almost immediately after injection and lasts for few hours, while effects of TM RNA delivered by antibody-LNP develops more slowly, reach a maximum at about 5 h after administration, and last for several days. We believe that these important and

expensive experiments deserve separate systematic studies in the near future. It is also tempting to think that these targeted interventions might optimize treatment of chronic diseases such as multiple sclerosis. However, at this early phase of VCAM-1 targeted drug delivery it seems more prudent and feasible to focus on proof of concept in acute settings, generally more amenable to use of targeted nanocarriers than chronic conditions.

Prior to the present study, these considerations lacked the solid basis of quantitative biodistribution data. Our systematic study in naïve mice and mice with acute brain inflammation yielded a most unexpected result: Targeting to VCAM affords not only exceptional selectivity but also sufficient capacity and cellular localization of drug delivery for therapeutic intervention stabilizing the leaky BBB in acute brain inflammation.

The differences in the brain targeting between different ligands (e.g., ICAM-1 vs. VCAM-1) most likely reflect differences in the exposure of these molecules in the luminal surface of the ECs rather than level of expression in the tissue. There may be a direct and even strong correlation between these two parameters in some cases, but numerous studies indicate that in a majority of vascular immunotargeting strategies accessibility to the targeted carriers circulating in the bloodstream is a more important parameter than tissue level of the target molecule (52, 65, 66).

In some key aspects, indeed, VCAM-1 and ICAM-1 have opposite targeting features. Uptake of anti-ICAM and anti-ICAM/agents in lungs exceeds that of anti-VCAM counterparts by orders of magnitude. In contrast, uptake in the inflamed brain of anti-VCAM formulations exceeds that of anti-ICAM counterparts by a similar margin. Interestingly, both VCAM-1 and ICAM-1 targeted agents show a similar increase in brain uptake when comparing control and injured animals, indicating that the superior cerebrovascular selectivity of VCAM-1 persists even in the presence of a significant increase in the expression and/or accessibility of both antigens. At the same time, vascular bed specificity is clearly not the only relevant consideration in targeting inflamed cerebral vasculature, as our results show clear superiority of anti-VCAM-1 over anti-TFR1 in this regard (*SI Appendix, Table S1*). To prove the therapeutic potential of VCAM-1 targeted LNPs, we used mRNA encoding for TM as a representative biomolecule that possesses anticoagulant and antiinflammatory functions. The findings raise a number of intriguing questions and avenues for future investigation.

Endogenous TM is thought to be nearly absent from the cerebral vasculature (67), and its functions following “artificial” introduction in this unusual environment will require further studies. Likewise, the fate of VCAM-1 targeted nanoparticles following binding to target antigen on activated brain ECs needs to be understood. Uptake of anti-VCAM-1 immunoliposomes has been studied in cultured ECs and reported to occur via

clathrin-mediated endocytosis (68), a pathway which would likely favor efficacy of anti-VCAM/LNP, but internalization and transport in vivo may be distinct or more complex. Likewise, carrier features such as size, shape, charge, and elasticity are likely to have significant impact on these processes (65, 66, 69). It is tempting to think that diverse drug delivery systems targeted to VCAM-1 will exert a distinct spectrum of these features. Alternative strategies such as adeno-associated virus with specificity to the BBB (70), brain shuttles [TfR, insulin receptor, glucose receptors, and LRP receptors (9, 12, 13, 71)], and TAT peptides (72) have been used to protect against the ischemia reperfusion injury, showing improvement of the BBB integrity in some cases.

In summary, this study opens multiple avenues for investigation of delivery, mechanism, and effects of a series of pharmacological agents targeted to the brain. Local and migrant constituents of CNS pathologies are immensely diverse, complex, and variable. Effective treatment of these pathologies cannot be afforded by a single drug delivery system, tested in any one animal model. For example, TNF injection in the striatum used in this study causes more widespread cerebral abnormalities than some alternative animal models, which have a more focal injury. Nearly complete normalization of this brain pathology attained by VCAM-targeted LNP/RNA encoding for TM implies that VCAM-1 targeting might find medical and investigational utility for site-specific pharmacological interventions in the inflamed brain.

Materials and Methods

Animal studies were carried out in accordance with the *Guide for the Care and Use of Laboratory Animals* (73) under protocols approved by University of Pennsylvania and Temple University Institutional Animal Care and Use Committees. Reagents, hybridomas, cell lines, modification of antibodies, preparation of immunoliposomes, radiolabeling of antibodies and immunoliposomes, immunoreactivity assays, intrastriatal TNF α model, radiotracing, autoradiography animal model of brain edema, brain disaggregation, flow cytometry and Western blot, targeted LNPs containing mRNA, biodistribution and luciferase transfection of targeted LNPs in vivo, TNF α model and intravital microscopy, and SPECT/CT imaging are described in *SI Appendix, Materials and Methods*.

Data Availability. All methods, protocols, reagents, and used sequences are described in detail in *SI Appendix*.

ACKNOWLEDGMENTS. V.R.M. received funding from NIH (Grants RO1 HL128398-02 and RO1 HL 143806-01) and Acuitas (SRA), V.R.M. and J.S.B. received funding from the Cardiovascular Institute of the University of Pennsylvania, O.A.M.-C. received funding from the American Heart Association (Grant 19CDA34590001), R.Yu.K. and P.M.G. received funding from NIH (Grant T32 HL 007971), and C.F.G. and L.R.W. received funding from NIH (Grant K08 HL130430). We acknowledge Kathleen LeForte for technical assistance in the preparation of this manuscript and Dr. Silvia Muro (University of Maryland) for the stimulating discussion of the manuscript.

- Danielyan, B.-S. Ding, C. Gottstein, D. B. Cines, V. R. Muzykantov, Delivery of anti-platelet-endothelial cell adhesion molecule single-chain variable fragment-urokinase fusion protein to the cerebral vasculature lyses arterial clots and attenuates post-ischemic brain edema. *J. Pharmacol. Exp. Ther.* **321**, 947–952 (2007).
- J. S. Brenner *et al.*, Red blood cell-hitchhiking boosts delivery of nanocarriers to chosen organs by orders of magnitude. *Nat. Commun.* **9**, 2684 (2018).
- C. Zhang *et al.*, Direct macromolecular drug delivery to cerebral ischemia area using neutrophil-mediated nanoparticles. *Theranostics* **7**, 3260–3275 (2017).
- N. L. Klyachko *et al.*, Macrophages with cellular backpacks for targeted drug delivery to the brain. *Biomaterials* **140**, 79–87 (2017).
- A. C. Anselmo *et al.*, Monocyte-mediated delivery of polymeric backpacks to inflamed tissues: A generalized strategy to deliver drugs to treat inflammation. *J. Control. Release* **199**, 29–36 (2015).
- D. Yuan *et al.*, Macrophage exosomes as natural nanocarriers for protein delivery to inflamed brain. *Biomaterials* **142**, 1–12 (2017).
- E. V. Batrakova *et al.*, A macrophage-nanozyme delivery system for Parkinson's disease. *Bioconjug. Chem.* **18**, 1498–1506 (2007).
- K. B. Johnsen, T. Moos, Revisiting nanoparticle technology for blood-brain barrier transport: Unfolding at the endothelial gate improves the fate of transferrin receptor-targeted liposomes. *J. Control. Release* **222**, 32–46 (2016).
- R. J. Boado, W. M. Pardridge, The Trojan horse liposome technology for nonviral gene transfer across the blood-brain barrier. *J. Drug Deliv.* **2011**, 296151 (2011).
- A. P. Fournier *et al.*, Prediction of disease activity in models of multiple sclerosis by molecular magnetic resonance imaging of P-selectin. *Proc. Natl. Acad. Sci. U.S.A.* **114**, 6116–6121 (2017).
- J. Hsu, J. Rappaport, S. Muro, Specific binding, uptake, and transport of ICAM-1-targeted nanocarriers across endothelial and subendothelial cell components of the blood-brain barrier. *Pharm. Res.* **31**, 1855–1866 (2014).
- M. Demeule *et al.*, Conjugation of a brain-penetrant peptide with neurotensin provides antinociceptive properties. *J. Clin. Invest.* **124**, 1199–1213 (2014).
- Y. Anraku *et al.*, Glycaemic control boosts glucosylated nanocarrier crossing the BBB into the brain. *Nat. Commun.* **8**, 1001 (2017).
- T. Sun *et al.*, Closed-loop control of targeted ultrasound drug delivery across the blood-brain/tumor barriers in a rat glioma model. *Proc. Natl. Acad. Sci. U.S.A.* **114**, E10281–E10290 (2017).
- M.-A. Bellavance, M. Blanchette, D. Fortin, Recent advances in blood-brain barrier disruption as a CNS delivery strategy. *AAPS J.* **10**, 166–177 (2008).
- G. H. Huynh, T. Ozawa, D. F. Deen, T. Tihan, F. C. Szoka, Jr, Retro-convection enhanced delivery to increase blood to brain transfer of macromolecules. *Brain Res.* **1128**, 181–190 (2007).

17. B. P. Mead *et al.*, Novel focused ultrasound gene therapy approach noninvasively restores dopaminergic neuron function in a rat Parkinson's disease model. *Nano Lett.* **17**, 3533–3542 (2017).
18. J. W. Seo *et al.*, Self-assembled 20-nm (64)Cu-micelles enhance accumulation in rat glioblastoma. *J. Control. Release* **220**, 51–60 (2015).
19. D. Yoo *et al.*, Core-cross-Linked nanoparticles reduce neuroinflammation and improve outcome in a mouse model of traumatic brain injury. *ACS Nano* **11**, 8600–8611 (2017).
20. M. D. Sweeney, Z. Zhao, A. Montagne, A. R. Nelson, B. V. Zlokovic, Blood-brain barrier: From physiology to disease and back. *Physiol. Rev.* **99**, 21–78 (2019).
21. A. S. Bonavia, M. R. McDevitt, M. J. Curcio, D. A. Scheinberg, Immunoreactivity assay for α -particle emitting monoclonal antibody constructs. *Appl. Radiat. Isot.* **64**, 470–474 (2006).
22. P. J. Hu, J.-F. Pittet, J. D. Kerby, P. L. Bosarge, B. M. Wagener, Acute brain trauma, lung injury, and pneumonia: More than just altered mental status and decreased airway protection. *Am. J. Physiol. Lung Cell. Mol. Physiol.* **313**, L1–L15 (2017).
23. P. Mattila, M. L. Majuri, P. S. Mattila, R. Renkonen, TNF alpha-induced expression of endothelial adhesion molecules, ICAM-1 and VCAM-1, is linked to protein kinase C activation. *Scand. J. Immunol.* **36**, 159–165 (1992).
24. A. Burke-Gaffney, P. G. Hellewell, Tumour necrosis factor-alpha-induced ICAM-1 expression in human vascular endothelial and lung epithelial cells: Modulation by tyrosine kinase inhibitors. *Br. J. Pharmacol.* **119**, 1149–1158 (1996).
25. H. Liu *et al.*, Label-free CEST MRI detection of citicoline-liposome drug delivery in ischemic stroke. *Theranostics* **6**, 1588–1600 (2016).
26. A. Montagne *et al.*, Ultra-sensitive molecular MRI of cerebrovascular cell activation enables early detection of chronic central nervous system disorders. *Neuroimage* **63**, 760–770 (2012).
27. M. Gauberti *et al.*, Ultra-sensitive molecular MRI of vascular cell adhesion molecule-1 reveals a dynamic inflammatory penumbra after strokes. *Stroke* **44**, 1988–1996 (2013).
28. N. Patel, B. A. Duffy, A. Badar, M. F. Lythgoe, E. Årstad, Bimodal imaging of inflammation with SPECT/CT and MRI using iodine-125 labeled VCAM-1 targeting micro-particle conjugates. *Bioconjug. Chem.* **26**, 1542–1549 (2015).
29. M. Fréchou *et al.*, Detection of vascular cell adhesion molecule-1 expression with USPIO-enhanced molecular MRI in a mouse model of cerebral ischemia. *Contrast Media Mol. Imaging* **8**, 157–164 (2013).
30. G. Llovera *et al.*, The choroid plexus is a key cerebral invasion route for T cells after stroke. *Acta Neuropathol.* **134**, 851–868 (2017).
31. S. Rom *et al.*, PARP inhibition in leukocytes diminishes inflammation via effects on integrins/cytoskeleton and protects the blood-brain barrier. *J. Neuroinflammation* **13**, 254 (2016).
32. N. A. Jessen, A. S. Munk, I. Lundgaard, M. Nedergaard, The glymphatic system: A beginner's guide. *Neurochem. Res.* **40**, 2583–2599 (2015).
33. C. Pösel, K. Möller, J. Boltze, D.-C. Wagner, G. Weise, Isolation and flow cytometric analysis of immune cells from the ischemic mouse brain. *J. Vis. Exp.* 53658 (2016).
34. B. S. Ding *et al.*, Anchoring fusion thrombomodulin to the endothelial lumen protects against injury-induced lung thrombosis and inflammation. *Am. J. Respir. Crit. Care Med.* **180**, 247–256 (2009).
35. C. F. Greineder *et al.*, ICAM-1-targeted thrombomodulin mitigates tissue factor-driven inflammatory thrombosis in a human endothelialized microfluidic model. *Blood Adv.* **1**, 1452–1465 (2017).
36. J. C. Murciano *et al.*, ICAM-directed vascular immunotargeting of antithrombotic agents to the endothelial luminal surface. *Blood* **101**, 3977–3984 (2003).
37. D. Weissman, K. Karikó, mRNA: Fulfilling the promise of gene therapy. *Mol. Ther.* **23**, 1416–1417 (2015).
38. N. Pardi *et al.*, Expression kinetics of nucleoside-modified mRNA delivered in lipid nanoparticles to mice by various routes. *J. Control. Release* **217**, 345–351 (2015).
39. X. Jiang *et al.*, Blood-brain barrier dysfunction and recovery after ischemic stroke. *Prog. Neurobiol.* **163–164**, 144–171 (2018).
40. O. Nicole *et al.*, The proteolytic activity of tissue-plasminogen activator enhances NMDA receptor-mediated signaling. *Nat. Med.* **7**, 59–64 (2001).
41. C. F. Greineder *et al.*, Dual targeting of therapeutics to endothelial cells: Collaborative enhancement of delivery and effect. *FASEB J.* **29**, 3483–3492 (2015).
42. H. Loghmani, E. M. Conway, Exploring traditional and non-traditional roles for thrombomodulin. *Blood* **132**, 148–158 (2018).
43. J. H. Griffin, B. V. Zlokovic, L. O. Mosnier, Activated protein C, protease activated receptor 1, and neuroprotection. *Blood* **132**, 159–169 (2018).
44. C. F. Greineder *et al.*, Vascular immunotargeting to endothelial determinant ICAM-1 enables optimal partnering of recombinant scFv-thrombomodulin fusion with endogenous cofactor. *PLoS One* **8**, e80110 (2013).
45. V. V. Shuvaev, J. S. Brenner, V. R. Muzykantov, Targeted endothelial nanomedicine for common acute pathological conditions. *J. Control. Release* **219**, 576–595 (2015).
46. M. Howard *et al.*, Vascular targeting of nanocarriers: Perplexing aspects of the seemingly straightforward paradigm. *ACS Nano* **8**, 4100–4132 (2014).
47. M. D. Howard *et al.*, Targeting to endothelial cells augments the protective effect of novel dual bioactive antioxidant/anti-inflammatory nanoparticles. *Mol. Pharm.* **11**, 2262–2270 (2014).
48. E. D. Hood *et al.*, Antioxidant protection by PECAM-targeted delivery of a novel NADPH-oxidase inhibitor to the endothelium in vitro and in vivo. *J. Control. Release* **163**, 161–169 (2012).
49. A.-M. Chacko *et al.*, Collaborative enhancement of endothelial targeting of nanocarriers by modulating platelet-endothelial cell adhesion molecule-1/CD31 epitope engagement. *ACS Nano* **9**, 6785–6793 (2015).
50. R. Y. Kiseleva *et al.*, Targeting therapeutics to endothelium: Are we there yet? *Drug Deliv. Transl. Res.* **8**, 883–902 (2018).
51. R. Y. Kiseleva *et al.*, Vascular endothelial effects of collaborative binding to platelet/endothelial cell adhesion molecule-1 (PECAM-1). *Sci. Rep.* **8**, 1510 (2018).
52. J. S. Brenner *et al.*, Mechanisms that determine nanocarrier targeting to healthy versus inflamed lung regions. *Nanomedicine* **13**, 1495–1506 (2017).
53. I. Papademetriou, Z. Tsinas, J. Hsu, S. Muro, Combination-targeting to multiple endothelial cell adhesion molecules modulates binding, endocytosis, and in vivo biodistribution of drug nanocarriers and their therapeutic cargoes. *J. Control. Release* **188**, 87–98 (2014).
54. D. N. Irani, D. E. Griffin, Regulation of lymphocyte homing into the brain during viral encephalitis at various stages of infection. *J. Immunol.* **156**, 3850–3857 (1996).
55. M. M. J. Poffliet *et al.*, Meningeal and perivascular macrophages of the central nervous system play a protective role during bacterial meningitis. *J. Immunol.* **167**, 4644–4650 (2001).
56. D. Sherman *et al.*; Enlimomab Acute Stroke Trial Investigators, Use of anti-ICAM-1 therapy in ischemic stroke: Results of the enlimomab acute stroke trial. *Neurology* **57**, 1428–1434 (2001).
57. J. Vuorte *et al.*, Anti-ICAM-1 monoclonal antibody R6.5 (Enlimomab) promotes activation of neutrophils in whole blood. *J. Immunol.* **162**, 2353–2357 (1999).
58. S. Wichert *et al.*, A single-arm, open-label, phase 2 clinical trial evaluating disease response following treatment with BI-505, a human anti-intercellular adhesion molecule-1 monoclonal antibody, in patients with smoldering multiple myeloma. *PLoS One* **12**, e0171205 (2017).
59. B. Rossi, S. Angiari, E. Zenaro, S. L. Budui, G. Constantin, Vascular inflammation in central nervous system diseases: Adhesion receptors controlling leukocyte-endothelial interactions. *J. Leukoc. Biol.* **89**, 539–556 (2011).
60. M. Nahrendorf *et al.*, 18F-4V for PET-CT imaging of VCAM-1 expression in atherosclerosis. *JACC Cardiovasc. Imaging* **2**, 1213–1222 (2009).
61. A. Tsourkas *et al.*, In vivo imaging of activated endothelium using an anti-VCAM-1 magneto-optical probe. *Bioconjug. Chem.* **16**, 576–581 (2005).
62. M. A. Bruckman *et al.*, Dual-modal magnetic resonance and fluorescence imaging of atherosclerotic plaques in vivo using VCAM-1 targeted tobacco mosaic virus. *Nano Lett.* **14**, 1551–1558 (2014).
63. R. Li *et al.*, Endothelium-targeted delivery of dexamethasone by anti-VCAM-1 SAINT-O-Somes in mouse endotoxemia. *PLoS One* **13**, e0196976 (2018).
64. V. R. Muzykantov, E. N. Atchina, H. Ischiropoulos, S. M. Danilov, A. B. Fisher, Immunotargeting of antioxidant enzyme to the pulmonary endothelium. *Proc. Natl. Acad. Sci. U.S.A.* **93**, 5213–5218 (1996).
65. J. W. Myerson *et al.*, Flexible nanoparticles reach sterically obscured endothelial targets inaccessible to rigid nanoparticles. *Adv. Mater.* **30**, 1802373 (2018).
66. J. W. Myerson *et al.*, Non-affinity factors modulating vascular targeting of nano- and microcarriers. *Adv. Drug Deliv. Rev.* **99**, 97–112 (2016).
67. H. Ishii, H. H. Salem, C. E. Bell, E. A. Laposata, P. W. Majerus, Thrombomodulin, an endothelial anticoagulant protein, is absent from the human brain. *Blood* **67**, 362–365 (1986).
68. M. Voinea, I. Manduteanu, E. Dragomir, M. Capraru, M. Simionescu, Immunoliposomes directed toward VCAM-1 interact specifically with activated endothelial cells—Aa potential tool for specific drug delivery. *Pharm. Res.* **22**, 1906–1917 (2005).
69. K. Müller, D. A. Fedosov, G. Gompper, Margination of micro- and nano-particles in blood flow and its effect on drug delivery. *Sci. Rep.* **4**, 4871 (2014).
70. G. K. Dogbevia *et al.*, Gene therapy decreases seizures in a model of Incontinentia pigmenti. *Ann. Neurol.* **82**, 93–104 (2017).
71. J. S. Kanodia *et al.*, Prospective design of anti-transferrin receptor bispecific antibodies for optimal delivery into the human brain. *CPT Pharmacometrics Syst. Pharmacol.* **5**, 283–291 (2016).
72. Y. Shi *et al.*, Endothelium-targeted overexpression of heat shock protein 27 ameliorates blood-brain barrier disruption after ischemic brain injury. *Proc. Natl. Acad. Sci. U.S.A.* **114**, E1243–E1252 (2017).
73. National Research Council, *Guide for the Care and Use of Laboratory Animals* (National Academies Press, Washington, DC, ed. 8, 2011).